Investigation of turbulent separation–reattachment flow in a curved-wall diffuser

Yin Jun-Fei and Yu Shao-Zhi
Department of Power Engineering, Nanjing Aeronautical Institute, Nanjing, Jiangsu Province, The People's Republic of China

A two-dimensional (2-D) laser velocimeter was employed to study the turbulent separation–reattachment flow field in a 2-D diffuser, which is a lower curved wall and upper flat plate. There is a parallel channel connected with the exit of the diffuser. In the inlet of the diffuser, the Reynolds number is 5,000 based on the momentum thickness, and the inlet velocity is 25.2 m/s. Mean velocity and Reynolds stresses were measured from upstream of the separation to downstream of the reattachment. The minimum distance from the surface is 0.3 mm. The significant features were that after transitory detachment, within the reversing flow, there exist the second extreme of $\overline{u^2}$ and minus of $-\overline{uv}$. Normal stresses and the cross-stream pressure gradient are important immediately in the separating flow and are associated with strong streamline curvature. The maximum of the displacement thickness curvature K^*_{max} corresponds to the intermittency transitory detachment. Several velocity profiles and Cebeci and Smith algebraic eddy-viscosity are compared with the experiment. A new approximate correction of the effect of normal stress is proposed and yields results in agreement with the experiment before the transitory detachment.

Keywords: turbulent boundary layer; separation flow; turbulence model; laser Doppler velocimeter; two-dimensional diffuser

Introduction

Turbulent boundary-layer separation often occurs in many fluid devices such as airfoils and diffusers. On the one hand, flow separation not only causes significant losses in the performance of the machines, but also leads to severe conditions in which the subsequent components operate. On the other hand, the separation of the shear layer may be followed downstream by reattachment of the separated layer to solid surfaces. Understanding the characteristics of the whole separation–reattachment flow process, therefore, becomes a significant problem in engineering applications.

Besides, turbulence is itself complex, and the problem becomes more difficult with flow separation and reattachment. Although many experiments have been done using well-established techniques such as hot-wires, the data on these are of little avail. The first reason is that the techniques lacked nondirectional sensitivity. The second is that the reversing flow is sensitive to the local blockage. The disturbance due to probes and their supports leads to a nonestimated error in measurement.

As a powerful technique of nonintrusive measurement, laser-Doppler velocimetry (LDV) is well suited to detect intermittent reversal flows. Since the 1980s, more and more researchers have favored investigating such kinds of flows with this technique. So far, most experiments with LDV have laid emphasis on the turbulent shear-layer separation on flat plates (Simpson 1981), trailing flap flows of airfoils (Nakayama 1985), or the reattached flow after the backward-facing step (Driver 1982). These research studies divided the whole flow into two research categories: separation and reattachment. Each basis flow was investigated individually. Experimental data with LDV that cover the whole detachment–reattachment are still lacking, except for Patrick's (1987) measurement of a flat-plate flow. In the present experiment, LDV was used to investigate a turbulent separation–reattachment flow field in a two-dimensional (2-D) curved-wall diffuser. The flows often take place with separation on a convex surface in internal flows, and therefore are usually more interesting to many engineers. This kind of flow provides a combined and basic situation against which many existing theories and models of turbulence can be tested and possibly improved.

The purpose of the present study is (1) to measure, in detail, flow characteristics in the separating, reattachment shear layers and reversal close to the solid surface, and (2) to obtain new experimental data for developing a new turbulence model.

Experimental arrangement

Experimental apparatus

This experiment was conducted in a low-speed suction open-circuit wind tunnel (Figure 1). The atmospheric air was

Address reprint requests to Professor Jun-Fei at the Department of Power Engineering, Nanjing Aeronautical Institute, Nanjing, Jiangsu Province, 210016, The People's Republic of China.

Received 2 April 1991; accepted 15 June 1992

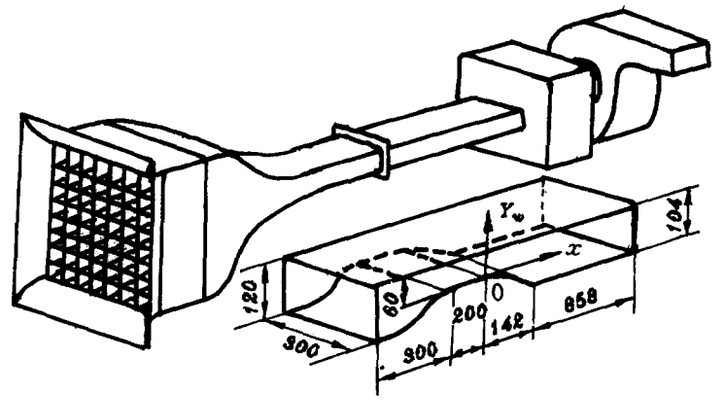

Figure 1 Experimental apparatus and test model

drawn into the test section after first passing through a plenum with a section of honeycomb and two screens of meshes, and was then accelerated by a contractive nozzle. At the exit of the test section, a large plenum was connected to prevent the disturbance from spreading upstream.

The test section is a 2-D convergent-divergent channel with the flat-plate roof. It consists of four segments: a convergent nozzle with a sine curve, a straight throat, a curved-wall diffuser, and a constant-area extended duct. The diffuser contour is approximately a circular arc. At the throat, the span-to-height ratio is 5. The exit-to-inlet ratio of the diffuser is about 1.73.

Measurement means and methods

The axes of the measurement coordinates were, respectively, parallel and vertical to the upper wall. $X = 0$ is located at the start of the diffuser. The origin of the Y-axis at each station was located at the local lower wall ($Y = 0$).

Fifty static pressure holes are spaced 5 mm apart on the floor from the inlet of the throat to the exit of the diffuser along the centerline. the lower turbulent boundary layer was tripped by a row of 1-mm-diameter wires with a screen at the entrance of the test section ($X = -500$ mm). In the constant throat ($X = -100$ mm), it has been developed as a reference shear layer.

A commercial two-color, four-beam LDV system (TSI Model-9100-7) was mounted on a three-dimensional (3-D) positioner to survey the whole shear-layer flow field for any selected increment of traverse from the model surface. The acquired data consisted of mean velocities, Reynolds stresses, and higher-order turbulence, etc. LDV was operated in the backward-scatter mode. An Argon ion laser with maximum power of 3 W provided intensity for particle-scattering light on the measurement. The effective frequency shifts from 10 KHz to 10 MHz were selected in both channels. In most of the measuring points, the effective frequency shift of 10 MHz was selected in order to detect high turbulence flows such as the separating flows.

The estimated signal-to-noise ratio from the TSI relationship is near 300. The two-channel counter processors of a TSI Model-1990B and a PDP-11-23 computer were used for data acquisition, analysis, and processing. Under the continue mode, the cycle number and the accuracy of comparison were, respectively, $N = 8$ and $\Delta = 1$ percent. The sample size was 3,840 for each measurement, and the validation data rates varied rapidly from 100 to 500 bursts per second over a distance of 3 mm from the wall. The window width of coincidence for both channels was set up with 30 μs to ensure that the two-channel signals came from the same scattering particle. Other coincidence window widths from 30 μs to 100 μs were also used to test, but these had no significant influence on the results.

Seeding was provided by a commercial liquid atomizer. Dioctyl phthalate particles (DOP) with a mean diameter of 0.54 μm was used as the scattering particles and was locally seeded at the entrance of the wind tunnel.

Overall uncertainties of the time-average velocities were carefully estimated according to error analysis and are presented in Table 1.

Notation

C_p	Pressure coefficient, $(p - p_{ref})/(0.5 * \rho * U_{ref}^2)$
H	Shape factor
p	Pressure
r_{pu}	Upstream–downstream intermittency
r_{puo}	Wall upstream–downstream intermittency
$\overline{u^2}$, $\overline{v^2}$, $-\overline{uv}$	Reynolds stress tensors
U, V	Mean component of velocity in the X and Y directions, respectively
X	Streamwise distance with origin at the start of the diffuser
Y	Distance from the lower wall and normal to the upper wall
Z	Span distance

Greek symbols

δ	Boundary layer thickness
δ^*	Displacement thickness
θ	Momentum thickness
ν_T	Eddy viscosity
ν_T^*	Nondimensional eddy viscosity
ρ	Density

Subscripts

e	Edge of boundary layer
w	Lower wall

Table 1 The uncertainties for the measurement results

	U	V	$\overline{u^2}$	$\overline{v^2}$	$-\overline{uv}$
Overall uncertainty	+0.383 −0.147	+0.225 −0.143	0.05 $(\overline{u^2})_{max}$	0.05 $(\overline{v^2})_{max}$	0.05 $(-\overline{uv})_{max}$

Near-wall measurement

The optical axis was tilted forward by 5° in the vertical plane to make measurement close to the surface. This means that the measured velocity components were not precisely equal to the vertical component. But the effect of inclination on vertical velocities is negligible ($\Delta V/V < 0.4$ percent), so no correction was made. The relative deviations of Reynolds stresses of v^2 and $-\overline{uv}$ are less than 5 percent of their true value. Therefore, the measured values were directly used.

The minimum distance from the surface for the measurement was 0.3 mm. The surface of the floor was coated with antireflection paint to reduce the scattering of lights by the wall. In the near-wall measurement, the signal gains were carefully controlled below a certain level such that the data rates become zero if either of a pair of incident beams was screened off. Although the noise level had been effectively suppressed by this treatment, the data rates were gradually decreased to 20–40 bursts per second. According to Cheround and Simpson's (1985) conclusion, the characteristic frequency of the energy-containing eddies is about $n_{max} = 125$ Hz for separating flows. Therefore, the present results in the near-wall region only contain the fluctuating information coming from the larger-eddy motions.

Experimental results

Test condition and two-dimensionality

When the reference station was at the position of $X = -100$ mm, the tripped shear layer developed as a typical 1/7 exponential profile. Those lower-wall boundary-layer parameters and free-stream conditions are also shown in Table 2.

The surface tuft observation was used to judge two-dimensionality and to roughly demarcate surface-flow regimes. The intermittent transitory detachment (ITD) is indicated as curved line; the central ITD is located near $X = 95$ mm and 1 mm downstream at 40 mm to either side.

LDV was used for the further check of two-dimensionality at the centerline ($Z = 0$) of the tunnel and $Z = \pm 30$ mm in $X = 95$ mm (near ITD). The results are shown in Figure 2. The two-side mean velocity components are a little larger than the central ones. The maximum differences are 0.03 and 1.8 percent of its free mean velocity. The two-dimensionality of the present test flow is basically satisfied.

Mean-flow results

The distribution of the flow parameters is shown in Figure 3. There is an acceleration between $X = -60$ mm and $x = 0$. C_{pw} and C_{pe} are always equal to or smaller than zero. The minimum value of $C_{pe} - C_{pw} = -0.041$ exists at $X = 0$. Obviously, the significant effect of wall curvature on the free-stream and surface pressures appears some 60 mm upstream of the start of wall curvature ($X = 0$). In Thompson and Whitelaw's (1985) separating flow, the free-stream pressure is not affected by the wall curvature. This is because the present ratio (0.011) of the displacement thickness to the wall radius is bigger than that (0.0092) of Thompson and Whitelaw's (1985) flow at the start of the curved wall. Therefore, the wall curvature plays a significant role in $X < 35$ mm of the present test flow.

Table 2 The reference inlet conditions at $x = -100$ mm

U_e	δ^*	H	$\sqrt{u^2}/U_e$	Re_θ
25.2 m/s	3.8 mm	1.325	0.50%	5000

The distribution of the surface downstream–upstream intermittency r_{puo}, at $X = 80$ mm, $r_{puo} = 0.99$, is the incipient point. At $X = 100$ mm, $r_{puo} = 0.80$, the intermittent transitory detachment. At $X = 120$ mm, $r_{puo} = 0.5$ is the transitory detachment (TD); here, $Cf = 0$. According to r_{puo}, the author gives five flow regions:

(1) the attached flow before the incipient detachment point (ID, $X < 80$ mm, $r_{puo} = > 0.99$),
(2) the intermittent detaching flow (80 mm $< = X < = 120$ mm, $0.5 < = r_{puo} = < 0.99$),
(3) the recirculating flow (120 mm $< = X < = 185$ mm, $r_{puo} < = 0.5$),
(4) the reattaching flow (185 mm $< = X < = 245$ mm, $0.5 < = r_{puo} < = 0.99$), and
(5) the relaxing flow ($X > = 245$ mm, $r_{puo} > = 0.99$).

The ratio of lengths of the intermittent detaching flow, the recirculating flow, and the reattaching flow is nearly 4:7:6. The reattaching flow length is 1.5 times that of the intermittent detaching flow. The reattachment needs a longer flow length because the reattachment exists under a nearly zero pressure gradient.

The other significant feature in Figure 3 is that $X = 95$ mm near ITD, and $C_{pe} - C_{pw}$ reaches its maximum value of 0.042. This feature is similar to Thomson and Whitelaw's flow (1985).

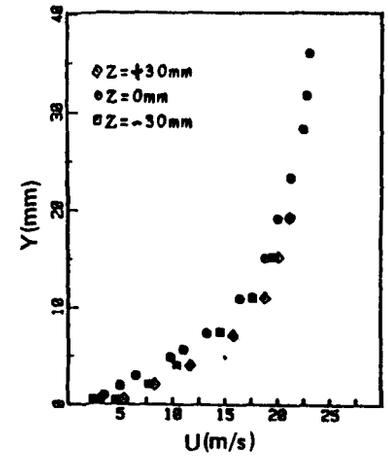

Figure 2 Two-dimensionality check

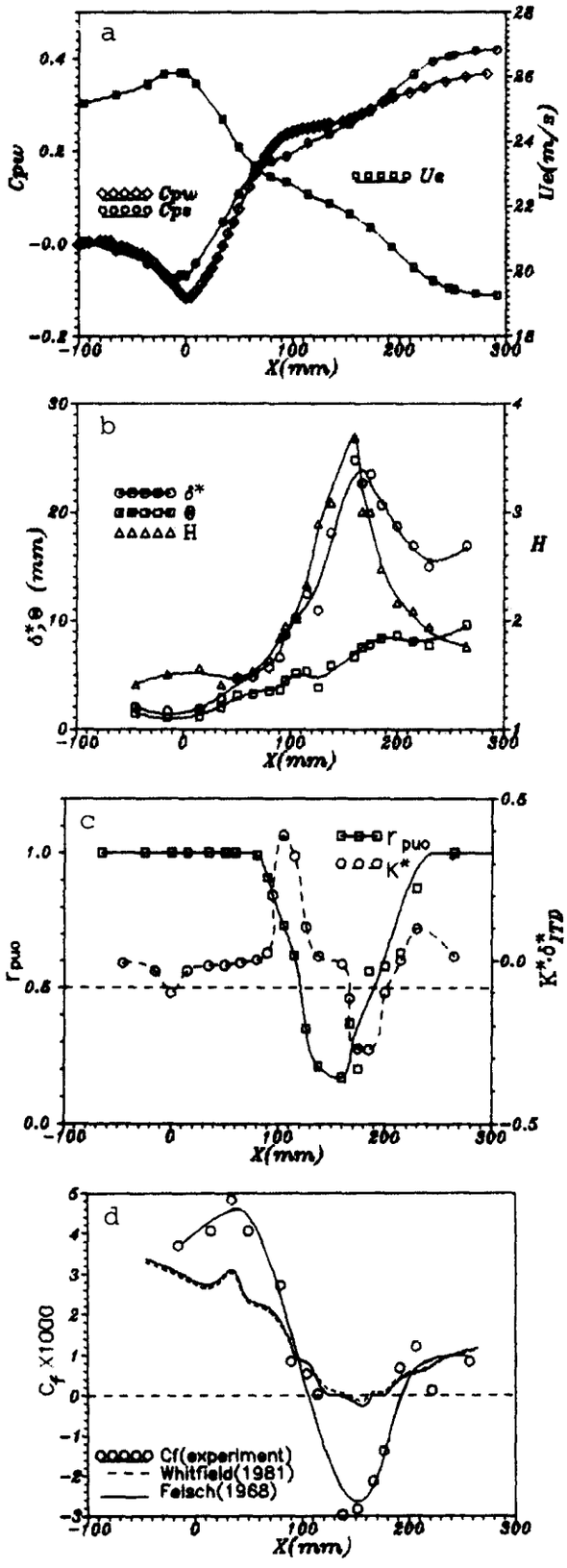

Figure 3 The distribution of flow parameters. (a) Pressure coefficient C_{pw}, C_{pe}, and free-stream velocity U_e; (b) integral parameters of H, δ^*, and θ; (c) upstream–downstream intermittency r_{puo} and displacement-thickness curvature K^*_{max}; (d) skin friction coefficient Cf

The boundary-layer separation produces a significant streamline curvature opposite to the walls and causes a strong normal pressure gradient in the present shear layer.

In Figure 3, the displacement-thickness curvature $K^* = K_w + d^2\delta^*/dx^2$ is calculated. K^* is the curvature for the effect inviscid-flow boundary. The normal pressure gradient is

$$\partial p/\partial y = -K^* \cdot \rho \cdot U_e^2 \tag{1}$$

At $X = 0$, $K^* < 0$ reaches the first minimum and there is a positive maximum of $C_{pe} - C_{pw}$. At $X = 95$ mm, K^* reaches the maximum and this maximum of $C_{pe} - C_{pw}$ is a negative number. In reattachment, this similar feature to the separation also exists.

The surface skin friction coefficient Cf was calculated by using the standard law of the wall to fit the near-wall velocity profile before ITD and after ITR, and by using the extrapolation of the total shear stress to the wall because of the nonvalidity of the logarithmic law of the wall in the detaching region. Other skin friction coefficients Cf calculated by using Felsch (1968) and Whitfield's (1981) relationship are also shown in Figure 3. The Felsch and Whitfield's Cf formulas are, respectively,

Felsch (1968):

$$Cf_{fe} = 0.058\ \mathrm{Re}_\theta^{-0.265}(0.93 - 1.95\log_{10}(H))^{1.705} \tag{2}$$

Whitfield (1981):

$$Cf_{wh} = 0.3\exp(-1.33H)/(\log_{10}(\mathrm{Re}_\theta))^{1.74+0.31H} + 1.1\times 10^{-4}(\tanh(4 - H/0.875) - 1) \tag{3}$$

$Cf = 0$ corresponds to TD ($X = 120$ mm) and IR ($X = 190$ mm), which are in agreement with $r_{puo} = 0.5$. In $X < 100$ mm, Cf is always greater than Cf_{fe} and Cf_{wh}, and in $X > 200$ mm Cf_{fe} and Cf_{wh} are in agreement with Cf. At the strong separating region, Cf_{fe} and Cf_{wh} differ from Cf. There is no significant difference between Cf_{fe} and Cf_{wh}, but Cf_{fe} could indicate a much smaller reversal, and $Cf_{fe} = 0$ is located downstream of $r_{puo} = 0.5$. Cf_{wh} is always greater than zero. The experience formula of Cf could be corrected continuously. Meanwhile, r_{puo} is a valid parameter to judge the turbulent separation rather than Cf.

The integral parameters of H and δ^* indicate a quick rise in separation. After ITD, δ^* almost increases linearly and in 70 mm $< X <$ 130 mm the line of δ^* is strongly curved, which gives significant streamline curvature near $X = 95$ mm, as shown in Figure 3. At ID, $\delta^* = 5.64$ mm and $H = 1.64$. At ITD, $\delta^* = 9.4$ mm and $H = 1.98$. At TD, $\delta^* = 16.5$ mm and $H = 2.3$. On $X = 160$ mm, the maximum shape factor, H reaches 3.68.

In reattachment, H and δ^* drops quickly. At IR, $X = 185$ mm, $\delta^* = 20.5$ mm, and $H = 2.5$. At ITR, $X = 215$ mm, $\delta^* = 17.6$ mm, and $H = 2.02$. At FR, $X = 245$ mm, $\delta^* = 15.5$ mm and $H = 1.83$.

Figure 4 illustrates the horizontal and vertical mean velocity components at the nondimensional height of Y/δ. The minimum horizontal velocity component is $-0.15U_e$, which occurs at $X = 138$ mm. The vertical components are always negative constants near the boundary-layer edge. In the reversal and near the surface, V/U_e is close to zero and even positive. In the reversal near $X = 138$ and 167 mm, V is larger than U. The maximum height of reversal is 4 mm, about 15 percent of the detached shear layer thickness. The length-to-height ratio of the reversal is 14.

Turbulence results

Figures 5, 6, and 7 show the profiles of Reynolds stress $\overline{u^2}$, $\overline{v^2}$, and $-\overline{uv}$. The maximums of $\overline{u^2}$, $\overline{v^2}$, and $-\overline{uv}$ have

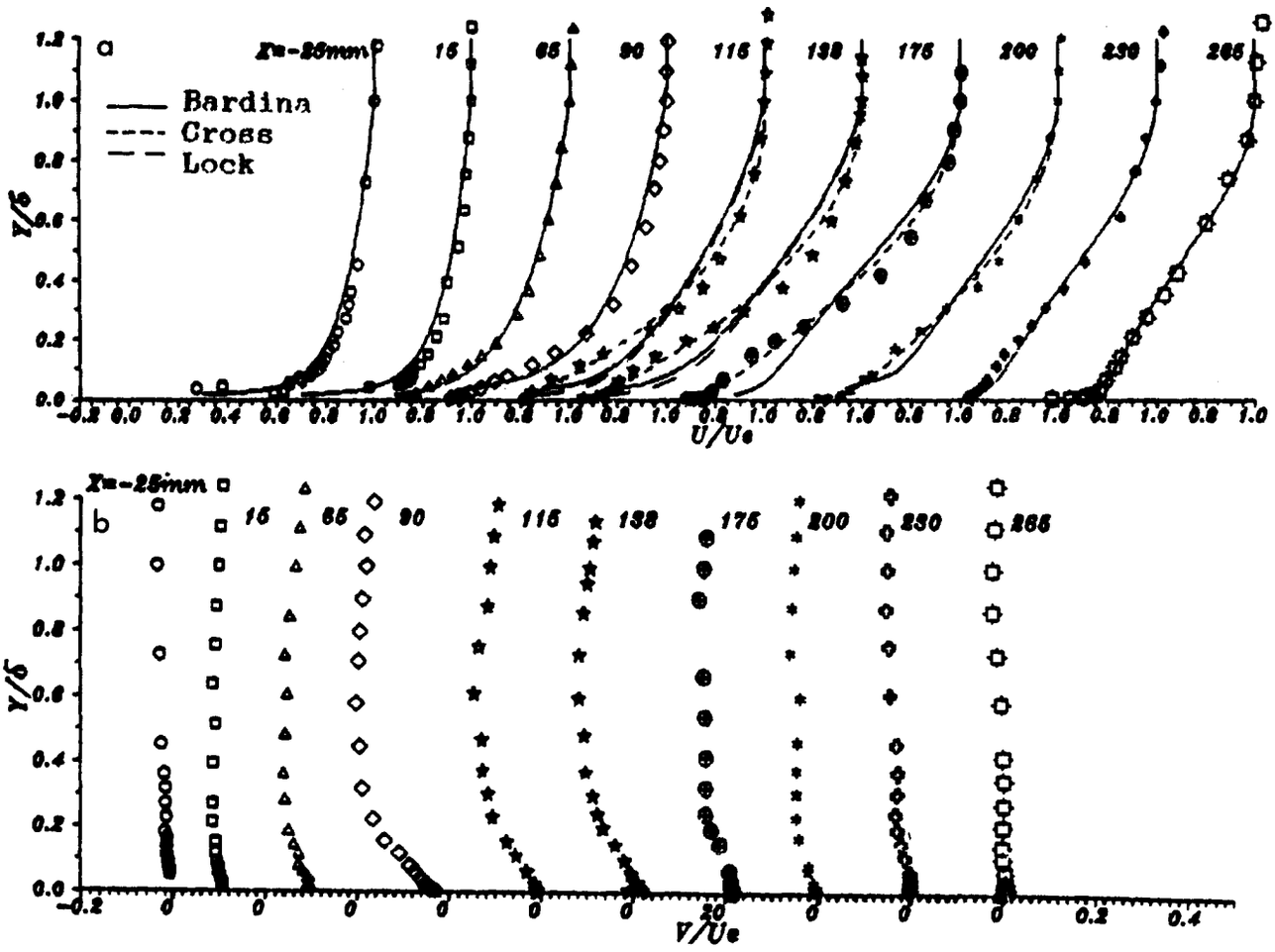

Figure 4 Velocity profiles. (a) Horizontal velocity profiles of U/U_e; (b) normal velocity profiles of V/U_e

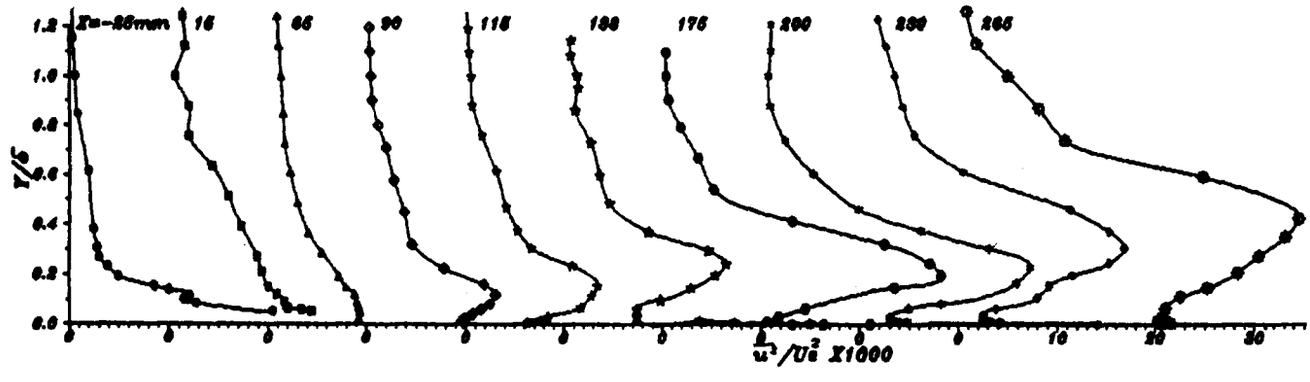

Figure 5 The profiles of Reynolds normal stress $\overline{u^2}$

almost the same height at a section. After ITD, its nondimensional height of Y/δ (= 0.2) is nearly constant along the streamwise direction.

In the profiles of Reynolds stresses, one of the most outstanding features is that a second extreme of $\overline{u^2}$ exists near the wall after the transitory detachment. But for $\overline{v^2}$, such a phenomenon is not obvious. Thompson and Whitelaw (1985) and Patrick (1987) also found this phenomenon. However, in Simpson's (1981) separating flow, there was this feature. It may be a characteristic of the recirculating flow, and it should be considered in turbulence modeling.

Another noticeable feature is that $-\overline{uv}$ appears negative in the backflow near the wall. The minimum of $-\overline{uv}$ corresponds to the smallest value of the downstream–upstream intermittency rpu at the same measuring section. This feature was not found for Simpson's (1981) flow, but it did exist in the trailing flow of airfoil (Thompson and Whitelaw 1985). Its mechanism is not clear. In the present flow, the negative extreme of $-\overline{uv}$ is almost the same as its

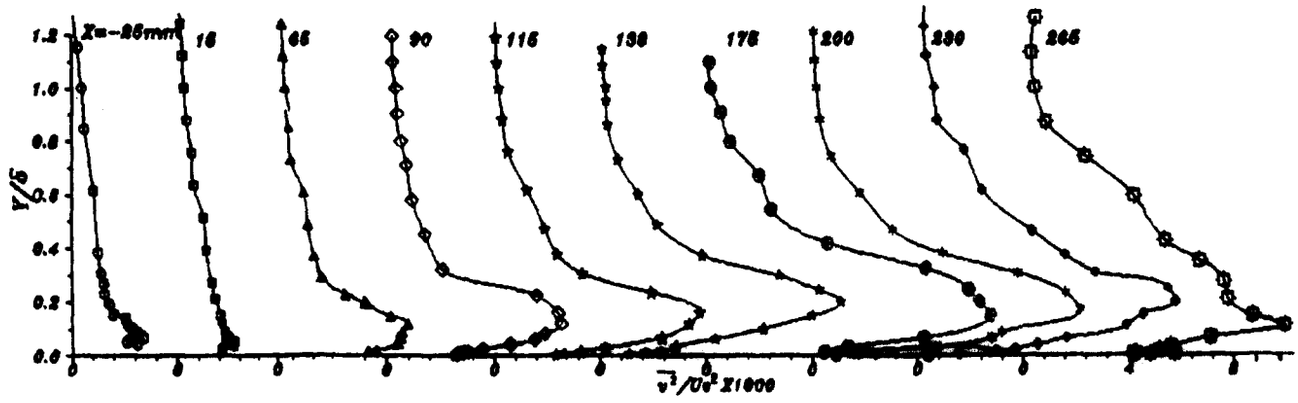

Figure 6 The profiles of Reynolds normal stress $\overline{v^2}$

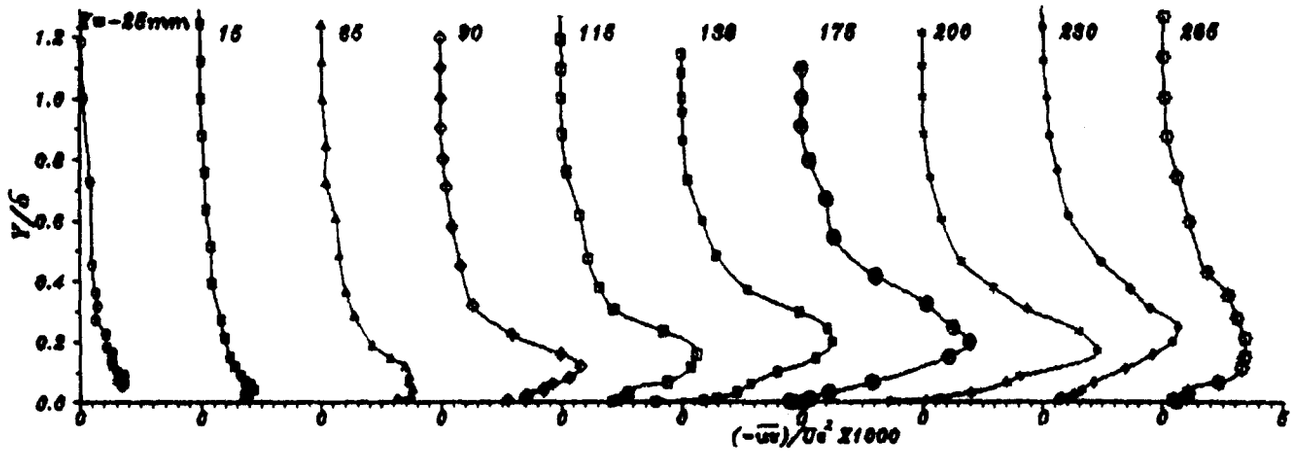

Figure 7 The profiles of Reynolds shear stress $(-\overline{uv})$

positive maximum in the magnitude. This may influence surface curvature.

Analysis of experimental results

The criterion for the separation

In Figure 8, the H vs. δ/δ^* path for the present data is shown according to the Sandborn–Kline (1961) separation criterion. From this criterion, $X_{ITD} = 120$ mm and $X_{ITR} = 180$ mm, no full separation is reached, and the corresponding length of the intermittency transitory detaching flow is reduced nearly by one half. The shape factors H at the ITD and ITR points are, respectively, lower than the predicted boundaries from Sandborn and Kline (1961). This means that the Sandborn–Kline criterion is still necessarily improved to agree with turbulent separation under conditions of fair or large curvature.

The streamwise variation of displacement thickness curvature K^* is shown in Figure 3. The extremum of K^* is located at $X = 95$ mm, $r_{puo} = 0.95$, which is rather near intermittent transitory detach ($X = 100$ mm, $r_{puo} = 0.8$). This feature also existed on other turbulent boundary-layer separating flows (Thompson and Whitelaw 1985; Nakayama 1985; Patrick 1987). K^* reflects the curvature of the displacement thickness boundary. K^*_{max} presents that the streamline is curved significantly in separation due to faster growth of the boundary layer. Therefore, authors suggest that K^*_{max} can be used as a new criterion to judge turbulent boundary-layer separation.

Mean velocity profiles

In Figure 4, Bardina (1981), Lock (1985), and Cross (1979) gave velocity profile relationships. Those velocity profiles take the following forms:

Bardina (1981):

$$U/U_e = 1 + V_T \mathrm{In}(\eta) - V_B \cos(\pi\eta/2) \quad (4)$$

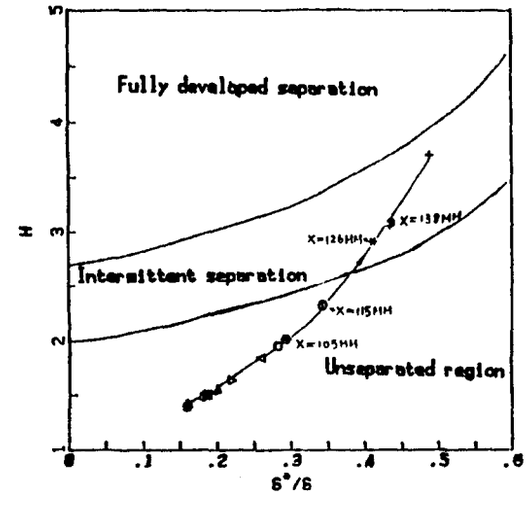

Figure 8 Sandborn and Kline (1961) separation criteria

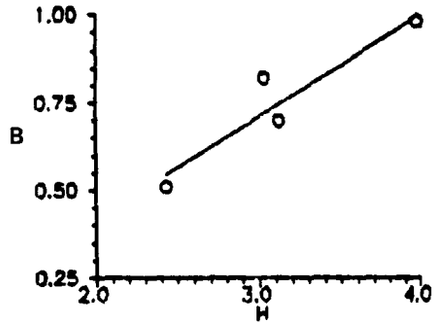

Figure 9 The relation of B and H

where $V_T = \sin(Cf)\sqrt{Cf/2}/K$, $K = 0.41$, $V_B = 2(\delta^*/\delta - V_T)$, and $\eta = y/\delta$. Bardina's profile is extended from Coles' velocity profile to the separated flow by using $V_T < 0$. When boundary layers separate, δ^*/δ is greater than 0.5, and H is generally greater than 4.

Lock (1985):

$$U/U_e = 1 + V_T \ln(\eta) - V_B F(\eta) \tag{5}$$

where $F(\eta)$ takes the form

$$F(\eta) = 1 \quad \text{if } 0 < \eta < \eta_z$$

$$F(\eta) = \{1 + \cos[\pi(\eta - \eta_z)/(1 - \eta_z)]\}/2, \quad \text{if } \eta_z < \eta < 1$$

Lock (1985) suggested that η_z should be taken as a function of δ^*/δ.

Cross (1979):

$$U/U_e = 1 + V_T \ln(\eta) - V_B\{1 - \sin^B(\pi\eta/2)\} \tag{6}$$

Obviously, $B = 2$, Cross' profile becomes Bardina's profile. Therefore, the wake's shape is corrected in Cross' profile with the variation of the parameter B.

Figure 4 shows that Bardina's profile could be in agreement with the present experimental results before ITD ($X < 100$ mm) and after ITR ($X > 200$ mm). But this profile could distinguish from the experiment in the recirculating flow (100 mm $< X <$ 200 mm).

In the recirculating flow, Cross and Lock's velocity profiles are used. Figure 4 shows that Lock's profile still differs from the experiment. The significant difference exists in $y/\delta > 0.3$ because the wake's shape could not reach the best fit. Cross's profile could fit the present experimental data well. But the value of B is set from 0.5 to 1 and less than $B = 2$ for the Coles' wake shape. With the increase of the shape factor H, B increases. To take H_{SEP} and B_{SEP} as 2.5 and 0.51, the relation between B and H is fitted as $B = B_{SEP} + 0.3(H - H_{SEP})$, shown in Figure 9. This relation is similar to Lock's relation (1985)

$$B = B_{SEP} + 0.1(H - H_{SEP}) \tag{7}$$

But the former's deflection is larger than the latter's. Lock's relation is from the separation flow of $H > 4$. The present flow shows the smaller shape factor, and H varies from 2.5 to 3.98. None of $H > 4$ exists.

Effects of normal stresses

The second-order Von Karman integral equation is

$$\frac{d\theta}{dX} + \frac{(H+2)\theta}{U_e}\frac{dU_e}{dX} = \frac{Cf}{2} + \frac{d}{dX}\left[\int_0^\delta (\overline{u^2} - \overline{v^2})\,dy\right]\Big/U_e^2 \tag{8}$$

The term on the left-hand side of Karman's equation is the second-order term, which presents the effects of normal stresses.

East (1979) gave the normal stress-correction relationship for the equilibrium attached flow in the following form:

$$I = \int_0^\delta (\overline{u^2} - \overline{v^2})/U_e^2\,dy = \mathrm{Qn}\,(H-1)\theta/H \tag{9}$$

where Qn = 0.072.

Hasting and Moreton (1982) and Hasting and William (1987) noticed that this correction gave smaller values than those in their experiments in the separated equilibrium layer and in the separating flow field near a NACA 4412 aerofoil at nearly maximum lift.

The present experiment results are integrated as

$$\mathrm{Qn} = I(\text{Experiment})H/[(H-1)\theta] \tag{10}$$

The results are shown in Figure 9. In $X < 120$ mm, Qn varies from 0.1 to 0.2, which is still larger than Qn = 0.072. After $X = 120$ mm, Qn grows quickly, the effects of normal stresses become more significant. A new correction could be investigated.

According to Gerhart's (1979) assumption of $(\overline{u^2} - \overline{v^2})/(-\overline{uv}) = 3.5$, which is supported by Simpson (1981), Reynolds shear stress could be presented by a turbulence model:

$$(-\overline{uv}) = \nu_T(\partial U/\partial Y)$$
$$(\overline{u^2} - \overline{v^2}) = 3.5(-\overline{uv}) = 3.5\nu_T(\partial U/\partial Y) \tag{11}$$

ν_T approaches Cebeci and Smith's (1977) algebraic eddy-viscosity in the outer layer:

$$\nu_T = 0.0168\delta^* U_e \quad \text{if } Y/\delta > 0.15 \tag{12}$$

For the inner layer,

$$\nu_T = (y/\delta)/0.15(0.0168\delta^* U_e) \quad \text{if } Y/\delta <= 0.15 \tag{13}$$

If we take the velocity gradient by using an approximate profile relationship given by Lock and Firman (1983),

$$U/U_e = 1 - 2/(H-1)[1 + \cos(\pi y/\delta)]/(3H) \tag{14}$$

If we integrate Equation 11 from the wall to the layer edge, we obtain

$$I = \mathrm{Qns}(H-1)\theta \quad \text{where Qns} = 0.0878 \tag{15}$$

The experimental Qns is set as I (experiment)/$[(H < 1)\theta]$ and shown in Figure 10. In $X < 150$ mm, Qns is in agreement with the present experiment. In $X > 150$ mm, Qns grows and is larger than 0.0878. Compared with Equation 9 as given by East

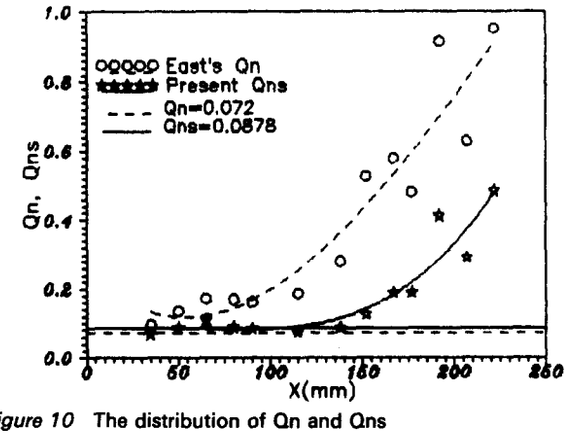

Figure 10 The distribution of Qn and Qns

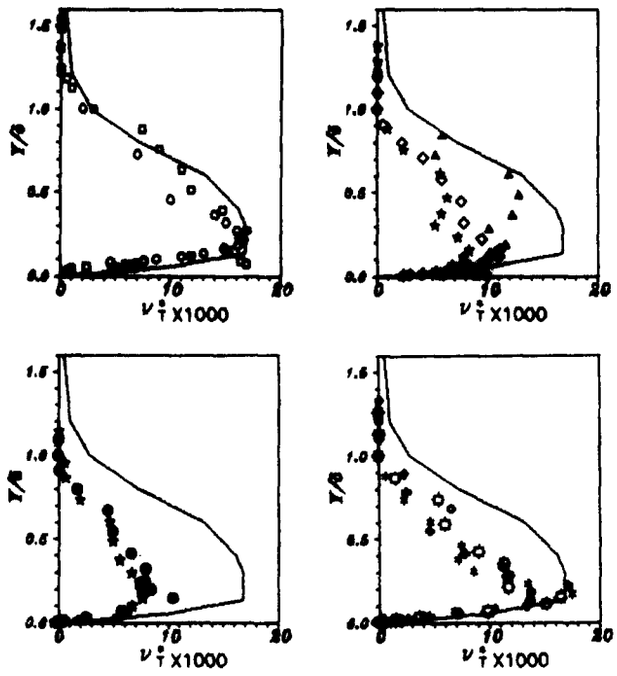

Figure 11 The profiles of eddy-viscosity ν_T^*. Solid line: Cebeci and Smith

(1979), the present relationship is better than East's (1979).

Eddy-viscosity

At present, the eddy-viscosity coefficient is commonly used in prediction:

$$(-\overline{uv}) = \nu_T(\partial U/\partial Y)$$
$$\nu_T^* = \nu_T/(\delta^* U_e) \tag{16}$$

In Figure 11, Cebeci and Smith's (C-S) (1977) algebraic model is compared with the experiment. In $X < 0$, the C-S model is in agreement with the experiment. In 60 mm $< X <$ 200 mm, the profiles of ν_T^* for the C-S model differ from the experiment significantly. It is remarkable that the eddy-viscosity becomes negative in the near-wall reversal. However, this negative eddy viscosity could never imply the reversal of energy from turbulence to mean flow. This is because there could be a significant production by the normal stresses (Nakayama 1984), and the diffusion of turbulence could balance with the generation (Simpson 1981).

Figure 12 presents the distribution of $\nu_{T_{max}}^*$ at the position of $(-\overline{uv})_{max}$. In $X < 0$, $\nu_{T_{max}}^* = 0.017$. After $X = 0$, $\nu_{T_{max}}^*$ decreases gradually. In 60 mm $< X <$ 200 mm, ν_{Tmax}^* is obviously smaller than the value 0.0168 used in the C-S model. With the development of the separation, ν_{Tmax}^* reduces to its minimum of 0.005 in X = 160 mm, which is half the size of the value 0.0168.

When the separated boundary layer started to reattach, $\nu_{T_{max}}^*$ also increased. In $X > 220$ mm, $\nu_{T_{max}}^*$ reaches 0.0168 in the equilibrium flow.

Conclusion

A 2-D LDV was used to survey a turbulent separation–reattachment flow field in a 2-D curved-wall diffuser. The minimum distance from the surface is 0.3 mm. According to

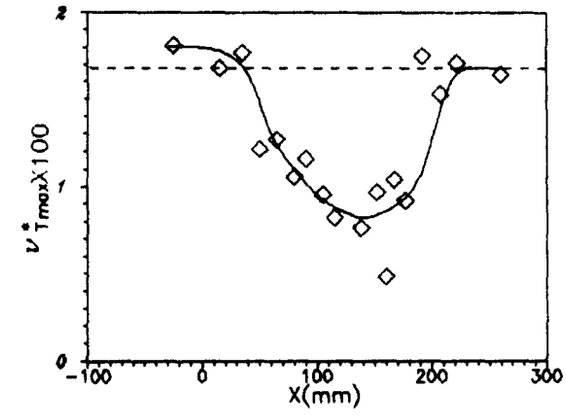

Figure 12 The distribution of $\nu_{T_{max}}^*$

the wall upstream–downstream intermittency, the whole flow can be divided into five regions: attached, intermittent detaching, recirculating, reattaching, and relaxing flow. The length ratio of reattaching to separating is 1.5. A second extreme of $\overline{u^2}$ and the minus of $-\overline{uv}$ appear near the wall after the transitory detachment. Reynolds normal stresses and a cross-stream pressure gradient are immediately important in the separation and are associated with strong streamline curvature. The maximum of the displacement thickness curvature K_{max}^* corresponds to the intermittency transitory detachment. Bardina's velocity profile could fit the experiment well before ITD and after ITR; its wake's shape is different from that of Coles. Cross' velocity profile could fit well the present experimental data from ITD to ITR. A new correction of the effect of the normal stresses on the Von Karman integral equation is suggested and yields results in agreeement with the present data. The Cebeci and Smith (1977) algebraic eddy-viscosity is not helpful in the separating flow.

References

Bardina, J., Kline, S. J. and Ferziger, J. H. 1981. A prediction method for planar diffuser flows. *ASME J. Fluids Eng.*, **103**, 315–321

Chehroudi, R. and Simpson, R. L. 1985. Space-time results for a separating turbulent boundary layer using a rapidly scanning laser anemometer. *J. Fluid Mech.*, **160**, 77–92

Cross, A. G. T. 1979. Calculation of compressible three-dimensional turbulent boundary layers with particular reference to wings and bodies. Report YAD3379, *Br. Aerospace*, Brough

Driver, D. M. and Seegmillier, H. L. 1982. Features of a reattaching turbulent shear layer subject to an adverse pressure gradient. *AIAA*, 82-0102, *AIAA/ASME 3rd Joint Thermophys. Fluids Plasma Heat Transfer Conf.*, June 7–11, 1982, St. Louis, MO

East, L. F., Sawyer, W. G. and Nash, C. R. 1979. An investigation of the structure of equilibrium turbulent boundary layers. RAE Technical Report 79040

Felsch, K. O., Geropp, D. and Walz, A. 1968. Method for turbulent boundary layer prediction. *1968 AFOSR-IFP-Stanford Conf.*, **1**, 170

Gerhart, P. M. 1979. An integral method for predicting subsonic turbulent separating boundary layers with specified free stream input. *ASME Turbulent Boundary Layer*, H. E. Weber (ed.), Pergamon Press

Hastings, R. C. and Moreton, K. G. 1982. An investigation of a separated equilibrium turbulent boundary layer. *Int. Symp. on Appl. L.D.A. to Fluid Mechanics*, Paper 11, Lisbon

Hastings, R. C. and Williams, B. R. 1987. Studies of the flow near a NACA 4412 aerofoil at nearly maximum lift. *Aeronaut. J.*, **91** (901), 29–44

Lock, R. C. and Firman, M. C. P. 1983. Survey of techniques for estimating viscous effects in external aerodynamics. *Proc. IMA*

Conf. Numer. Methods Aeronaut. Fluid Dynamics, P. Roc (ed.). Academic Press, New York

Lock, R. C. 1985. Velocity profiles for two-dimensional turbulent separated flows. *Boundary-Layer Separation*, F. T. Smith and S. N. Brown (eds.). IUTAM Symposium London, 1986; Springer-Verlag, Berlin and Heidelberg, 1986

Nakayama, A. 1984. Measurements of attached and separated turbulent flows in the trailing-edge regions of airfoil. *Proc. Symp. Numer. Physical Aspects of Aerodynamic Flows*, T. Cebeci (ed.), **2**, 233–258

Nakayama, A. 1985. Measurements of separating boundary layer and wake of an airfoil using laser doppler velocimeter. *AIAA*, 85–0181, AIAA 23rd Aerospace Sci. Mtg., Jan. 14–17, 1985, Reno, NV

Patrick, W. P. 1987. Flowfield measurements in a separated and reattached flat plate boundary layer. NASA CR-4052

Sandborn, V. A. and Kline, S. J. 1961. Flow model in boundary-layer stall inception. *ASME J. Basic Eng.*, **83**, 317–327

Simpson, R. L., Chew, Y. T., and Shivaprasad, B. G. 1981. The structure of a separating turbulent boundary layer. *J. Fluid Mech.*, **113**, 23–74

Thompson, B. E. and Whitelaw, J. H. 1985. Characteristics of a trailing-edge flow with turbulent-layer separation. *J. Fluid Mech.*, **157**, 305–326

Whitfield, D. L. 1981. Calculation of turbulent boundary layers with separation and viscous-inviscid interaction. *AIAA J.*, **19** (10), 1315–1322